Zn-Al layered double hydroxide-based nanocomposite functionalized with an octahedral molybdenum cluster exhibiting prominent photoactive and oxidation properties

T.K.N. Nguyen, L.Y. Matsui, Naoto Shirahata, N. Dumait, Stéphane Cordier, Fabien Grasset, N. Ohashi, Tetsuo Uchikoshi

*

Zn-Al layered double hydroxide-based nanocomposite functionalized with an octahedral molybdenum cluster exhibiting prominent photoactive and oxidation properties

Ngan Thi Kim Nguyen[1,2], Yoshio Matsui[1], Naoto Shirahata[3], Noée Dumait[4], Stéphane Cordier[4], Fabien Grasset[1,2,4], Naoki Ohashi[1,2] and Tetsuo Uchikoshi[1,2*]

1) Research Center for Functional Materials, National Institute for Materials Science (NIMS), 1-2-1 Sengen, Tsukuba, Ibaraki 305-0047, Japan

2) CNRS–Saint-Gobain–NIMS, UMI 3629, Laboratory for Innovative Key Materials and Structures (LINK), National Institute for Materials Science, 1-1 Namiki, Tsukuba, Ibaraki 305-0044, Japan

3) Research Center for Materials Nanoarchitectonics (MANA), National Institute for Materials Science (NIMS), 1-1 Namiki, Tsukuba 305-0044, and Japan

4) Univ. Rennes, ENSCR, INSA Rennes, CNRS, ISCR (Institut des Sciences Chimiques de Rennes) – UMR 6226, F-35000 Rennes, France

Corresponding author:

Tetsuo UCHIKOSHI

Full postal address: Research Center for Functional Materials, National Institute for Materials Science (NIMS), 1-2-1 Sengen, Tsukuba, Ibaraki 305-0047, Japan

Telephone: +81-29-859-2460 / Fax: +81-29-859-2401

E-Mail address: UCHIKOSHI.Tetsuo@nims.go.jp

Thi Kim Ngan NGUYEN
Full postal address: Research Center for Functional Materials, National Institute for Materials Science (NIMS), 1-2-1 Sengen, Tsukuba, Ibaraki 305-0047, Japan
E-Mail address: NGUYEN.Thikimngan@nims.go.jp

Abstract

A new layered double hydroxide (LDH)-based nanocomposite functionalized with an octahedral molybdenum atom cluster (MC) exhibiting prominent photoactive and oxidation properties was synthesized. Zn-Al LDH and Zn-Al LDH intercalated dodecyl sulfate compounds (abbreviated as LDH-1 and LDH-2 respectively) were prepared by the co-precipitation method in an aqueous solution. The MCs were simply introduced into the LDH-2 by an anion exchangeable method in dimethylformamide under ambient conditions. The extension of the basal spacing of the LDH-1 from 0.9 nm to about 5 nm by intercalating dodecyl sulfate and Mo_6 cluster was confirmed by several complementary technics. The octahedral structure of the Mo_6 cluster was retained after the modification process in an organic dispersing medium that was confirmed by ultraviolet-visible absorption and photoluminescence experiments. The possible chemical bonding between the $[Mo_6Cl^i_8Cl^a_{6-x-y}(H_2O)_x(OH)^a_y]^{x-2}$ (x = 0, 1 or 2 and y = 0, 1, 2, 3 ; x + y = 3) clusters and LDH-2 was suggested on the basis of by X-ray photoelectron spectroscopy. The excellent photoactive and oxidation performance of the Mo_6 cluster on the methylene blue degradation in an aqueous solution was determined in the dark, under UV light (λ =370 nm) or with the existence of H_2O_2. The combination of the LDH-2 with a high absorbability and recyclability and the Mo_6 cluster will be a

promising candidate as a heterogenized homogeneous catalyst for removing organic pollutants.

KEYWORDS: molybdenum, octahedral cluster, outer surface functionalization, layered double hydroxide, photochemistry, pollutant degradation

1. INTRODUCTION

Among the various wastewater treatment techniques, the adsorption has been proposed as one of the best methods due to its inexpensiveness, universal nature, and ease of operation. Many studies have paid attention to determining new functional and large-scale productive materials for removing organic pollutants by adsorption combined with photocatalytic degradation [1]. This approach becomes an important pathway for pharmaceutical contaminant removal that attracts huge interests of the studies based on TiO_2, ZnO, or graphene-functionalized materials [2, 3]. Besides, layered double hydroxides (LDH) are well known as important compounds due to their interlayer anion exchangeability and potential material for industrial-scale applications such that their fundamental understanding in heterogeneous catalysis, water treatment, and drug delivery is developed [4-5]. LDH with the general formula of $[M^{2+}_{1-x}M^{3+}_{x}(OH)_2]^{x+}[A^{n-}]_{x/n}\cdot mH_2O$ (x as the molar ratio $M^{2+}/(M^{2+} + M^{3+})$ in the range 0.2–0.33) is composed of the divalent and trivalent metals occupying at the octahedral center [6]. The positive charges on the metal hydroxide layers are generated by the exchange of the divalent metals (Cu, Zn, Co, Mg, Cr…) by the trivalent metals (Al, Fe, Tb…) and it is neutralized by negatively exchangeable organic or inorganic ions (A = NO_3^-, CO_3^{2-}, SO_4^{2-}, F^-, Cl^- or alkyl anions…) accompanied by the absorption of the interlayer water

molecules [7-12]. The remarkable advantages of the LDH are made of relatively inexpensive and safe elements, highly adjustable, and easily synthesized that becomes good advantages for industrial-scale applications. The physicochemical characteristics could be controlled by the flexible exchange of the chemical components of the metal hydroxide-based layer or the functionalization of the exchangeable interlayer ions. Based on the host lamellar structure and ionic exchangeable possibility, LDH has been widely studied in applicable fields such as absorbents [12], prominent photoactive catalysts [13, 14], energy conversion and storage [15], and drug delivery systems [16-18], as a result of the modification of the trivalent metal. Moreover, the efficiency of the catalytic characteristics of the LDH has been highlighted to study the organic reactions such as aldol condensation [19], ethanol electro-oxidation [20], and dinitrogen fixation [21]. Most of the cases depend on the catalytic possibility of the functional groups existing between the ionic metal hydroxide layers. Particularly, single-atom Au-intercalated NiFe LDH, Ce-doped MgAl LDH functionalized Au nanoparticles, or polyoxometalate-intercalated LDH have revealed the optimal achievements for catalytic applications [22-24].

The improvement of the typical physicochemical characteristics or enhancement of the active sites by adjusting the interlayer trivalent or divalent metals of the LDH as well as exchanging a functionalized interlayer component was widely investigated. However, the challenge to figure out a suitable synthesis depends on the intrinsic property and size of the functional-controlling substances. In this study, the $Cs_2Mo_6Cl_{14}$ (CMC) clusters compound, with excellent redox and optical properties, has been selected as a catalytic functionalized group to combine with the LDH. As is known, the basic concept of metal atom cluster (MC) was first introduced by F. A. Cotton in 1964 to define a finite group

of the metal atoms (two or more) that are held together by metal-metal bonds and surrounded by other nonmetal ligands [25]. Typically, the octahedral MC (M_6) composed of the $\{M_6L^i_8\}^{4+}$ (M = Mo, W, Re) metallic cores (L^i = inner ligand) coordinating with apical ligands (L^a = Cl, Br, I or $OCOC_nF_{2n+1}$) exhibits strong absorption in both the ultraviolet (UV) and visible light ranges, resulting in a prominent luminescent emission within the deep red/near-infrared (NIR) region [26-29]. In the reduced form, the valence electron concentration (VEC) is equal to 24 electrons per the $[M_6L^i_8L^a_6]^{2-}$ cluster unit that visibly displays a redox characteristic for the catalyst application [30-32]. As previously reported, the excitation state of MC produces singlet oxygen ($^1O_2$) with a strong catalytic activity for the photoreduction applications has been investigated [33]. However, the Mo_6 cluster in the bulk powder state is limited in the applicability as well. Graphene oxide or h-BN are ones of the excellent candidates to enhance the photocatalytic applicability of the Mo_6 cluster has a proven highly catalytic efficiency for the hydrogen production from water [34], water purification [35], synthesis of dimethyl carbonate from CO_2 and methanol [36] or photoreduction of carbon dioxide into methanol [37]. A remarkable study has been progressing to simultaneously combine the gold nanoparticles and the Mo_6 cluster on the graphene oxide resulting in an excellent photoactive possibility for the degradation of rhodamine B under visible light irradiation [38]. A few studies have continued to determine efficient supporting materials for the catalytic-characterized MC with the expectation to fabricate the heterogeneous nanostructured composite for photovoltaic, nanobiotechnology, or energy-saving fields [27, 28].

The goal of this study is to focus on the photoactive and oxidation properties of the MC on dye degradation after combined with an LDH neutral supporting material with only

high absorbability and recyclability. Indeed, among LDH, Zn/Al LDH (abbreviated as LDH-1) exists a weak basic catalyst, and Zn also was the limiting species for the photocatalytic reaction [39]. It was almost used as an efficient absorbent and/or support for multifunctional catalysts. In this work, the new nanocomposite (abbreviated as Mo_6@LDH-2) was prepared by the delamination of Zn_2Al LDH co-intercalated dodecyl sulfate (abbreviated as LDH-2) in dimethylformamide and then introducing the as-synthesized $[Mo_6Cl^i_8Cl^a_6]^{2-}$ cluster units. The initial octahedral structure of the Mo_6 cluster was not modified after incorporation into the LDH, as confirmed by the optical properties. The Mo-O-Al/Zn chemical bonding between the Mo atoms of the $\{Mo_6Cl^i_8\}^{4+}$ anion cluster core and the LDH was validated. The new Mo_6@LDH-2 nanocomposites were successfully fabricated by a quick, cheap, and reproducible method with high and stable efficiency of the Mo_6 cluster units. Moreover, we have demonstrated the catalytic activity of the Mo_6 cluster anion intercalated in the LDH on the methylene blue.

2. MATERIALS AND METHODS

2.1 Materials

The $Zn(NO_3)_2.6H_2O$ (99%) and $Al(NO_3)_3.9H_2O$ (98%, pH= 2~4) were supplied from Chameleon Reagent. Sodium n-dodecyl sulfate ($CH_3(CH_2)_{10}CH_2OSO_3Na$) was purchased from the Kanto Chemical Company. The sodium hydroxide (NaOH, 5 mol/L) was purchased from Nacalai Tesque. All chemicals were used without purification. The deionized water with the conductance of $0.5.10^{-4}$ S/m was obtained using Water Purifiers WG710 equipment at 25°C.

142

143 *2.2 Methods*

144 *Preparation of LDH-1 and LDH-2*

145 LDH-1 and LDH-2 were prepared by the co-precipitation method with the Zn and Al
146 ratio of about 2 [7, 40]. Fixed amounts of the $Zn(NO_3)_2{\cdot}6H_2O$ (0.02 mol) and
147 $Al(NO_3)_3{\cdot}9H_2O$ (0.01 mol) salts were simultaneously dissolved in 50 ml of deionized
148 water and agitated by a magnetic stirrer for 1 h to obtain a homogeneous solution.
149 Similarly, the transparent mixture solution containing the $Zn(NO_3)_2{\cdot}6H_2O$ (0.02 mol),
150 $Al(NO_3)_3{\cdot}9H_2O$ (0.01 mol) and sodium dodecyl sulfate (SDS) (0.01 mol) in 50 ml of
151 deionized water was used for the preparation of the LDH-2. The aqueous solution of
152 NaOH (5 M) was then used to titrate the mixed salt solution until the pH value reached
153 10. The solution was then agitated for 24 h at room temperature to increase the
154 crystallinity of the LDH. The precipitated product was purified by deionized water
155 several times until the pH was about 7. The collected solid powder was dried at 60^oC for
156 24 h for further use.

157

158 *Synthesis of Mo_6@LDH-1 and Mo_6@LDH-2 nanocomposites*

159 The CMC cluster unit was prepared according to a procedure already reported that
160 combined the use of solid-state and solution chemistries [41, 42]. LDH-1 or LDH-2 (0.3
161 g) was dispersed in 140 ml of dimethylformamide (DMF) by ultrasonication for 1 h.
162 The yellow CMC cluster powder (0.06 g) was similarly dissolved in 60 ml of DMF
163 solution by ultrasonication. LDH-1 or LDH-2 and CMC cluster solutions were then
164 mixed and continually agitated for 24 h to improve the intercalation. The yellow-
165 colored product was separated and washed with DMF to eliminate the residual Mo_6

cluster, then dried at 60^{o}C for 24 h for further characterizations. The experimentally determined wt. % concentration of the CMC cluster powder in the Mo_6@LDH-1 and Mo_6@LDH-2 nanocomposite was about 16.7 wt.%.

2.3 Catalytic test

The catalytic activity of the LDH and Mo_6@LDH samples was characterized by measuring the degradation possibility of methylene blue (MB) in an aqueous solution. The difference in the catalytic activity and adsorption-desorption isotherm was evaluated through the tests for LDH-2 and Mo_6@LDH-2 (catalyst/MB = 20). The investigation was performed on the solution containing 20 mg of a catalyst in 10 ml of MB solution (20 mg/L) (catalyst/MB = 100) at room temperature without or with i) the addition of the H_2O_2 solution (5% in ethanol, Sanwa Chemical Co., Ltd.), ii) irradiation of ultraviolet (UV) light (λ = 370 nm) or iii) in the presence of both H_2O_2/UV system. A source of the UV light was generated by a 300 W Xenon lamp (MAX-303, Asahi Spectra Co., Ltd.). The MB degradable efficiency of the filtered catalyst-mixed MB solution was confirmed by the UV-Vis absorption spectroscopy (V-650, Jasco). The C/C_o index was calculated based on the intensity ratio of the optical absorption peak at 664 nm of MB with and without the existence of the catalyst. The catalytic reaction rate and the effect of H_2O_2 concentration on the degradation reaction of MB with and without the UV light were investigated. For comparison, the catalytic test of the CMC cluster alone was also carried out at the same Mo_6 cluster concentration (16.7 wt%) in the Mo_6@LDH-2 nanocomposite.

2.4 Characterizations

The average hydrodynamic diameters and distribution of the LDH-2 and Mo_6@LDH-2 powders in water were measured by an ultrafine particle analyzer (Nanotrac NPA151 - Nanotrac ULTRA, Microtrac Inc., USA) incorporated the controlled reference method (CRM) in a dynamic light scattering instrument. The crystalline layered structure of the samples was determined by powder X-ray diffraction (XRD) (SmartLab, RIGAKU, 40 kV and 30 mA) in the 2θ angle range from 1° to 50° for the bulk powder at the scan speed of 1/ min with the Cu Kα radiation (λ = 1.54 Å). The optical absorbances of the powders were measured by UV-Vis-NIR spectroscopy (V570, Jasco Corp.) in the wavelength range of 220 to 2000 nm at the scan rate of 400 nm/min. Emission spectra of the powder were obtained by high-performance fluorescence spectroscopy (JASCO FP8500) connected to a Xenon lamp at the scan rate of 500 nm/min. The surface morphology and the elemental composition were analyzed by field emission scanning electron microscopy (FE-SEM, S4800, Hitachi High-Technologies Corp.) at 10 kV coupled with an energy-dispersive X-ray (EDX) analysis device. High-resolution observations of the powder were performed by a high-resolution transmission electron microscopy (HRTEM) (JEOL JEM 2100F) equipped with an EDX analysis device. Inductively coupled plasma optical emission spectrometry (ICP-OES, Agilent 720-ES) coupled with ion-chromatography (Thermofisher Scientific ICS-1600) was used to verify the element concentration. The typical chemical vibrations of the samples were verified by Fourier transform infrared spectroscopy (FTIR) (Thermo scientific Nicolet 4700) in the wavenumber range from 4000 to 400 cm^{-1}. The nitrogen adsorption isotherm according to the BET model of the LDH-2 and Mo_6@LDH-2 nanoparticles was performed in saturated vapor pressure of about 100 kPa at the temperature of 140^{o}C for 2 days (BELSORP-max II, Microtrac BEL Corp.). Thermogravimetric analysis

(TGA) and differential thermal analysis (DTA) were carried out using a TG/DTA 6200 apparatus (SII, EXSTAR 6000, Hitachi, Japan) operated in an N_2 atmosphere at the heating rate of 10/min. The electron binding energy spectra within the CMC and Mo_6@LDH-Zn/Al were measured by X-ray photoelectron spectroscopy (XPS) (PHI Quantera SXM (ULVAC-PHI)) using Al Kα radiation at 20 kV and 5 mA and taken off the angle of 45^o. All binding energies were calibrated concerning the C 1s peak of the adventitious carbon at 285 eV.

3. RESULTS AND DISCUSSION

Figure 1a shows the powder XRD patterns of the as-synthesized LDH-1, Mo_6@LDH-1, LDH-2, and Mo_6@LDH-2 powders, and the characteristic peaks are observed. The LDH-1 exhibits the typical characteristic of the LDH phase assigned to structure I. The characteristic diffraction peaks (indexation in bracket) are located at 2θ angles of 11.6^o (003), 23.4^o (006), 34.5^o (009) and 39^o (015), 46^o (018) corresponding to the basal planes as claimed in previous reports [43]. Besides, the remarkable patterns of the ZnO phase formed on the brucite-like sheets were also verified with the peaks at the 2θ angles of 32^o, 34^o, and 36^o in this study [43]. In the case of Mo_6@LDH-1, it shows the same lamellar structure with LDH-1 without the change in the XRD peak positions. The basal plane spacing value of the 003 planes calculated by Bragg's law for LDH-1 is about 0.9 nm which is too narrow to intercalate the CMC clusters with a size of 1.2 nm [42]. For this reason, the dodecyl sulfate (DS) anion was selected to expand the space of the metal hydroxide layers in LDH-1 to form LDH-2. The XRD result of LDH-2 illustrates that a new series of reflections of the (003), (006) and (009) planes of LDH-2 simultaneously appear at the lower 2θ angle assigned to structure II and the d_{003} spacing

value increases from 0.9 to 2.7 nm. In addition, LDH-2 still retained the original layered structure as seen for structure I in LDH-1. This result confirmed the partial exchange of NO_3^- anions by the 2 nm-sized dodecyl sulfate anions as seen in previous reports [43, 44]. Very interestingly, the intercalation in the CMC cluster causes a significant reduction of peak intensity assigned to structure II of LDH-2 as seen in the XRD pattern of Mo_6@LDH-2. It could be suggested that a part of the DS intercalated LDH, which is mixed with the Mo_6 cluster, becomes a poorly crystallized phase, or undergoes exfoliation. Good interaction between the DMF molecules and dodecyl sulfate anions is efficient to expand the basal space between the brucite-like layers of LDH-2 that assists in the movement and intercalation of the Mo_6 cluster during the intercalation step. The average hydrodynamic diameters and distributions of LDH-2 and Mo_6@LDH-2 in water are displayed in **Figure S1**. The average hydrodynamic diameter of LDH-2 reduces from 0.5980 µm to 0.2815 µm for Mo_6@LDH-2 corresponding to the broader size distribution. This result is agreeable with the crystallinity reduction of the LDH phase as claimed in the XRD pattern, resulting in a partial exfoliation. The BET surface areas of LDH-2 of about 50.0 m^2/g and Mo_6@LDH-2 of about 20.4 m^2/g were evaluated by the nitrogen adsorption isotherm (**Fig. S2a**). The shape of the nitrogen adsorption isotherm curves of LDH-2 and Mo_6@LDH-2 is almost similar to the characteristic of the LDH. That proves the retention of the layered structure of the LDH in Mo_6@LDH-2 after the partial exfoliation as suggested in the XRD pattern. The decrease of the adsorbed volume agrees with the pore diameter distribution in **Figure S2b** which shows the significant reduction of the small pore size in the range below 20 nm. The schematic representation of the process to fabricate the LDH and the possible structure of its nanocomposite based on the XRD pattern are illustrated in **Figure 1b**.

The HRTEM image of Mo_6@LDH-2 shows black areas assigned to the aggregated Mo_6 cluster anion (**Fig. 2a**). In the beginning, the CMC cluster dissociates in the solvent to form the Cs^+ cations and $[Mo_6Cl^i_8Cl^a_6]^{2-}$ anions. Moreover, it is well known that the $[Mo_6Cl^i_8Cl^a_6]^{2-}$ anion is able to quickly exchange apical Cl ligands by water molecules or hydroxyl anions to obtain $[Mo_6Cl^i_8Cl^a_{6-(x+y)}(H_2O)^a_x(OH)^a_y]^{x-2}$ ($x + y \leq 6$) clusters [45]. Indeed, the interlayer galleries of LDH are containing water molecules and hydroxyl for balancing the positively charged surface, which can react with the apical Cl ligands. Following a theoretical suggestion, we can assume that only the Mo_6 anion or neutral compound can adsorb or deposit on the positive metal hydroxide surface of the LDH, so in that case x = 0 or 1 and y = 0 to 5.

The layer structure of Mo_6@LDH-2 is confirmed in the STEM image and the calculation of the basal spacing distance of about 5 nm as seen in Figures **2b and 2c**. STEM-EDX mapping of the Mo_6@LDH-2 nanocomposite confirms the existence of Mo and Cl atoms as presented in **Figure 2d**.

In order to confirm the stability of the octahedral structure of the Mo_6 cluster in Mo_6@LDH-2, the optical properties of the reflectance and the photoluminescence were evaluated. It could be seen that LDH-1 and LDH-2 show a high optical absorption below 400 nm while Mo_6@LDH-2 is composed of the adsorbing part of the Mo_6 cluster below 400 nm and the LDH below 370 nm (**Fig. 3a**). This result confirms the retention of the octahedral Mo_6 structure on the LDH. In **Figure 3b**, LDH-1 and LDH-2 normally possess no photoluminescence in the NIR range while the Mo_6 cluster shows a strong emission at 700 nm in the deep red/NIR region. However, the photoluminescent intensity of the Mo_6 cluster is not strong in the spectrum of Mo_6@LDH-2, this is due to the significant change in the apical halogen ligand of the CMC cluster. As known, the

photoluminescent property of the Mo_6 cluster is decreased when the apical halogen ligands are replaced by H_2O molecules or hydroxyl anion [32, 41, 45].

The chemical bonding of the prepared compounds was verified by FT-IR spectroscopy presented in **Figure 4**. In the FT-IR spectrum of LDH-1 appears a strong peak at 1385 cm^{-1} that indicates for the NO_3^- linking existing in the basal spacing of the LDH. In addition, the vibrational bands for Zn-O at 427 cm^{-1}, Zn-OH at 608 cm^{-1} of the brucite-like layers, O-H bending at 1650 cm^{-1} and O-H stretching at the broadband of 3450 cm^{-1} of the free inter-lamellar water molecules are observed. The FT-IR spectrum of LDH-2 shows the vibrational bands assigned to the dodecyl sulfate: i) C-H stretching vibrational band of CH_2 at 2928 cm^{-1} and CH_3 at 2854 cm^{-1} from the alkyl chain and ii) asymmetric stretching vibrational band at 1220 cm^{-1} and symmetric stretching vibrational band at 1059 cm^{-1} originating from the OSO_3^- group [43]. The vibrational signal of NO_3^- at 1385 cm^{-1} in LDH-2 decreases after exchanged by DS anions. The FT-IR spectrum of Mo_6@LDH-2 would be composed of the vibrational band of the LDH-2 and Mo_6 clusters. Following the typical band intensity for DS, the concentration of DS is obviously reduced by an exchange of the Mo_6 cluster. It should be noted that new peaks appear at 1654 cm^{-1} that were properly related to the O-H bending vibrational band of the H_2O free molecules with strong hydrogen bonding [46] as recognized in the report of the $[Mo_6Br^i_8Br^a_6]^{2-}$ cluster [47]. From this result, the hydrogen bonding could be created between apical groups of the $[Mo_6Cl^i_8Cl^a_{6-(x+y)}(H_2O)^a_x(OH)^a_y]^{x-2}$ clusters and the free interlayer-adsorbed water molecules in the LDH.

Figure 5 shows the TG, DTG, and DTA results of the LDH-1, LDH-2, and Mo_6@LDH-2. The total mass loss was respectively, figured to be about 40 wt. %, 50 wt. % and 46 wt. % for LDH-1, LDH-2, and Mo_6@LDH-2 after heating to 800^oC. The

thermogravimetric behavior (DTG) shows the mass loss with four steps in the temperature range of 50-200 ^{o}C, 200-300 ^{o}C, 300-500 ^{o}C and 500-800^{o}C for LDH-1, 50-150, 150-250, 250-400 and 400-800^{o}C for LDH-2, and 50-150, 150-320, 320-600 and 600-800^{o}C for Mo_6@LDH-2. The weight loss in the first step indicates the release of the interlayer water molecules adsorbed on the surface of the Zn^{2+}/Al^{3+} ionic brucite-like layers. Dehydroxylation and thermal degradation of the counter anion is realized at the second decomposing step and, simultaneously, metal oxidation occurs with the dehydroxylation of the brucite-like layers. The complete dehydroxylation occurs in the temperature range of 500-800^{o}C that destroys the brucite-like structure of the LDH. In the last step, all the counter anions, which are strongly adsorbed on the metal oxide crystallites, would be removed.

The DTA curves of LDH-2 almost display only an exothermic event because of the quick decomposition of the dodecyl sulfate during the beginning steps. In contrast, the DTA results of LDH-1 and Mo_6@LDH-2 show a similar endothermic event in the second thermal decomposing step. In this step, the phase transformation starts to occur and accelerates the melting process to destroy the crystallinity of the brucite-like layers in the third decomposition step. In Mo_6@LDH-2, the surfactant concentration was significantly reduced that did not affect the decomposition as seen in LDH-2. In the third and fourth degradation steps, the performance of the metal oxide from the dihydroxylation of the brucite-like layers also enhances the enthalpy of the thermal event that linearly increases the endothermic value [43]. Interestingly, in the third degradation step of the DTA curve of Mo_6@LDH-2, a clearly enhanced endothermic peak appears at 450 ^{o}C due to the formation of molybdenum oxide caused by the destruction of the Mo_6 octahedral structure.

Figure 6a summarizes the XPS spectra of the CMC and Mo_6@LDH-2. All the binding energies were calibrated concerning the C1s peak of the adventitious carbon at 285 eV. The binding energies of the Zn, Al, C, O, Cs, Mo, Cl, and S elements in the CMC and Mo_6@LDH-2 powders are listed in **Table S1**. Interestingly, the Cs element was not found in Mo_6@LDH-2, as presented in **Figure 6a**. As already explained, in the solvent, the CMC cluster dissociated to 2 Cs^+ and 1 $[Mo_6Cl^i_8Cl^a_6]^{2-}$ ions and the Cs^+ cation can be kept by the exchangeable anion adsorbed on the LDH or Cl- from CMC, which was removed through the washing step. The binding energies of Zn 2p and Al 2p are respectively assigned by the two peaks at 1022.3 eV ($2p_{3/2}$) and 1045.4 eV ($2p_{1/2}$) and a peak of 74.7 eV that agrees with a previous study [48]. The dodecyl sulfate component is confirmed by the appearance of the binding energy of the S2p at the peak of 169.1 eV. It is important to verify the difference in the binding energy of the Mo and Cl components in the Mo_6 cluster after intercalated into the LDH.

In **Figure 6b**, the Mo3d XPS spectrum of the CMC cluster shows peaks at 229.7 eV ($3d_{5/2}$) and 232.8 eV ($3d_{3/2}$) assigned to the Mo^{2+} cation from the $[Mo_6Cl_{14}]^{2-}$ cluster [36]. In the XPS spectrum of Mo_6@LDH-2, the Mo3d binding energy is recognized by the peaks at 229.7 eV ($3d_{5/2}$) and 232.6 eV ($3d_{3/2}$) related to the Mo_6^- cluster [49, 50, 51]. Interestingly, one new peak at 234 eV ($3d_{3/2}$) indicating Mo-O appears in the Mo_6@LDH-2 compound. It could be proof for the interaction between the Mo atom from the Mo_6 cluster and O atom from the hydrotalcite layers of the LDH to form the Mo-O-Zn or Mo-O-Al bonding. This behavior has been also claimed by Haiping Li et al. for the Zn(Al)–O–Bi(Mo) bonds between the Bi_2MoO_6 groups and Zn/Al-LDH [52]. Moreover, the O1s XPS spectrum of Mo_6@LDH-2 shows a peak at 530.9 eV indicating O-Mo bonding that was not confirmed in the XPS spectrum of the CMC cluster as

expected (**Tab. S1**). In addition, the binding energy assigned to the O1s of CMC with a peak at 532.6 eV that is verified for the freely absorbed water molecules (**Tab. S1**) while the binding energy of O1s of Mo_6@LDH-2 is also characterized by a peak at 530.9 eV which indicates the O-Zn, O-Al, or O-Mo bonding.

Similarly, the XPS spectrum of the CMC cluster for the Cl2p including three clear peaks at 198.3 eV ($2p_{3/2}$), 200.4 ($2p_{3/2}$), and 200.2 ($2p_{1/2}$) while only one broad peak was observed for the Cl2p for Mo_6@LDH-2 (**Fig. 6c**). To distinguish the inner and apical Cl ligands, the spectrum deconvolution of the Cl2p region was performed for the XPS spectra of the Cl2p of CMC cluster and Mo_6@LDH-2, as listed in Table 2. The deconvolution spectrum of the Cl 2p region of the CMC cluster shows four peaks at 198.25, 199.85, 200.39 and 201.99 eV that indicate $Cl^{(a)}2p_{3/2}$, $Cl^{(a)}2p_{1/2}$, $Cl^{(i)}2p_{3/2}$ and $Cl^{(i)}2p_{1/2}$, respectively (**Fig. 6d and Tab. 1)** [53]**.** For Mo_6@LDH-2, the XPS deconvolution of the Cl2p shows the same peaks at 198.25 eV ($Cl^{(a)}2p_{3/2}$), 199.85 eV ($Cl^{(a)}2p_{1/2}$), 201.35 ($Cl^{(i)}2p_{3/2}$), and 201.95 eV ($Cl^{(i)}2p_{1/2}$) which are properly related to Mo-Cl of the $[Mo_6Cl^i_8Cl^a_6]^{2-}$ anion (**Fig. 6e**). The ratio $Cl^{(a)}2p$/ $Cl^{(i)}2p$ was experimentally calculated to be 5.8/8 for the $[Mo_6Cl^i_8Cl^a_6]^{2-}$ anion in the CMC cluster and 3.6/8 for the $[Mo_6Cl^i_8Cl^a_{6-(x+y)}(H_2O)^a_x(OH)^a_y]^{x-2}$ anion in Mo_6@LDH-2. This deconvolution agrees with an analysis of the XPS spectra as mentioned in Table 1, following the average loss of at least three apical Cl ligands on the Mo_6 anion in Mo_6@LDH-2. All these results support for the possible chemical bonding between the $[Mo_6Cl^i_8Cl^a_3(OH)^a_3]^{-2}$ or $[Mo_6Cl^i_8Cl^a_3(H_2O)^a(OH)^a_2]^{-1}$ anionic clusters or $[Mo_6Cl^i_8Cl^a_3(H_2O)^a_2(OH)^a_1]$ neutral cluster and the hydroxide of ZnAL LDH. Very interestingly, new peaks of the Cl2p were noted in the deconvolution spectrum at 198.9 eV ($2p_{3/2}$) and 200.5 eV ($2p_{1/2}$) that suggested the energy bonding of Cl with another

metal (Zn or Al) [48]. It could be explained that the apical Cl^- anions separated from the Mo_6 cluster by exchange with the interlayer water molecules will directly adsorb on the positively charged hydrotalcite surface of the LDH. Aiming to clarify the quantitative analysis of the element components of Mo_6@LDH-2, an ICP-OES analysis was performed that indicated the ratio of Zn, Al, and Mo atoms of about 1.96, 1.00, and 0.38. The Mo element definitely existed in the Mo_6@LDH-2 at a significant concentration as well as confirmed in the STEM-EDX mapping image. The ratio between the Cl and Mo atoms in Mo_6@LDH-2 indicated by ICP-OES analysis was 2.23 (the theoretical ratio is 2.33) which means almost all the original Cl (from ligands) still exist in the nanocomposite after treatment. This result suggests too that a part of the Cl^- could be directly adsorbed on the LDH.

As known, the H_2O_2/UV or H_2O_2/catalyst systems are widely used in advanced oxidation technology, one of the most environmentally friendly techniques to degrade pollutants [54]. In this study, the efficiency of the MB degradation caused by the Mo_6 cluster deposited on LDH with and without UV and H_2O_2 or both as a radical generating source. **Table S2** and **Figure 7** present the change in the C/Co value that was calculated from the optical absorbance (664 nm) of the samples and blank illustrated in **Figure S3**. First, the evaluation of the MB adsorbing possibility of LDH-2 and Mo_6@LDH-2 was performed by stirring with MB aqueous solution (catalyst/MB = 20/1) for 72h in the dark (**Fig. S3a**). The intensity of the adsorbing peak at 664 nm assigned to MB significantly decreased by about 80 wt% caused by Mo_6@LDH-2, meanwhile, it is 66 wt% for LDH-2. Considering the BET surface area of LDH-2 of about 50.0 g/m^2 and Mo_6@LDH-2 of about 20.4 g/m^2 (**Fig. S2**), the adsorbing possibility of the Mo_6@LDH-2 should be lower than that of LDH-2. That means a part of the degraded MB is caused

406 by the oxidation reaction of the Mo_6 cluster. To clarify this phenomenon, the Mo_6 cluster,
407 LDH-2, Mo_6@LDH-2 powders were dispersed in the MB solution (catalyst/MB = 20/1)
408 in the dark, with UV or H_2O_2 or both of them for 2 h (**Fig. S3b and c**). The calculated
409 C/Co value of all samples was presented in **Figure 7a** and **Table S2**.
410 In **Figure 7a**, the decrease in the degraded MB concentration caused by the CMC
411 cluster was recorded at 57% in the dark, at 98% with UV or H_2O_2 that proved strong
412 oxidation and photoactive properties of the Mo_6 cluster [30, 31]. As a result,
413 Mo_6@LDH-2 also displays the MB degrading efficiency that is 71 wt% in dark and
414 96% with H_2O_2. Their MB degrading possibility slightly reduce in the irradiation of the
415 UV light for the same catalyst. This result is proof for the advantage of the intercalation
416 of the Mo_6 cluster on the LDH in comparison with LDH that shows the degraded MB
417 concentration at 54% in the dark and 65% with H_2O_2. Barras et al. reported the
418 photocatalytic degradation of rhodamine B over $[Mo_6Br_8(N_3)_6]^{2-}$ cluster units under
419 sunlight irradiation with catalyst/rhB ratio of 1/1 for 2 h [38]. Besides, Ivanova et al.
420 also claimed the efficient photocatalyst of the hexamolybdenum cluster supported on
421 exfoliated hexagonal boron nitride (h-BN) nanosheet with the catalyst/rhB ratio of
422 100/1 [35]. In comparison, the H_2O_2/Mo_6@LDH system also shows a catalytic
423 efficiency with the catalyst/MB ratio of 100/1 even in the dark.
424 For the first time, the combination of the Mo_6 cluster and H_2O_2 was performed to test
425 the oxidation reaction on dye degradation and it shows excellent results. Only H_2O_2 is
426 unable to degrade the MB cations. H_2O_2 is suggested as an effective agent accelerating
427 for the Mo_6 cluster in the initial step of the MB degradation process.
428 **Figure 7b and 7c** illustrate the degradation rate and effect of the H_2O_2 concentration on
429 the catalytic activity of the H_2O_2/Mo_6@LDH-2 with and without UV (λ=370 nm) light

illumination as well as the change in the solution color as seen in **Figure S4**. The tested suspensions were collected every 30 minutes from the original suspension for 210 minutes. The catalytic activity for the MB degradation decreases when the H_2O_2 concentration is increased. For this result, a suitable amount of H_2O_2 for the 20 mg catalyst to obtain the optimal catalytic activity is recorded at 0.3 mM in both cases with and without UV light illumination. The rate of the MB degradation by the H_2O_2/ Mo_6@LDH-2 is also confirmed with the strong reduction of the MB concentration for the first 30 min that includes the absorption of MB on the surface of the LDH. The pH increases, which is recorded during light irradiation, suggests the appearance of hydroxyl anions during the initial and propagating reactions. Moreover, the chemically component modification of the Mo_6@LDH-2 nanocomposite after the reaction with MB in the presence of the H_2O_2 solution was measured by FTIR spectroscopy as seen in **Figure S5**. The vibrational band assigned to the NO_3^- group was significantly decreased accompanying a decrease in the O-H vibrational band assigned to the free H_2O molecules that prove the use of interlayer-absorbed H_2O_2 molecules for the degradation reaction of MB. Nevertheless, the XRD patterns of the Mo_6@LDH-2 before and after the test with the MB degradation show no change as seen in **Figure S6**. That means the layered structure of LDH is not modified and the degradation of the MB almost occurs mostly on the outside surface of the Mo_6@LDH-2 nanosheets. In addition, the MB degradable possibility by Mo_6@LDH-2 was observed for the concentration reduction of about 66% for the second recycling run.

In summary, the non-photochemical reactions for the degradation of MB based on the Mo_6@LDH-2 nanocomposite is suggested by the following equations [36, 37, 38, 55].

(Eq.1) H_2O_2 + (Mo_6 cluster) → (Mo_6 cluster) (h^+) + $^{\cdot}OH$ + OH^-

(Eq.2) (Mo_6 cluster) + hν → (Mo_6 cluster) (h^+, e-)

(Eq.3) (Mo_6 cluster)(h^+) + H_2O → (Mo_6 cluster) + $^{\cdot}OH$ + H^+

(Eq.4) (Mo_6 cluster)(e^-) + O_2 → (Mo_6 cluster) + $O_2^{-\cdot}$

(Eq.5) H_2O_2 + hν → $2\,^{\cdot}OH$

(Eq.6) $H_2O_2 + O_2^{-\cdot}$ → $^{\cdot}OH + {}^{-}OH + O_2$

(Eq.7) $H_2O_2 + {}^{\cdot}OH$ → $^{\cdot}O_2H + H_2O$

The Mo_6 cluster plays an important role as an electron supplying source for the initial reaction with the strong support of H_2O_2 to generate free radicals as seen in Eq. 1. The radical generating process is less efficient when the Mo_6 cluster is excited by UV light because of taking two steps as depicted by Eq. 2 and Eq. 3 to form hydroxyl radicals ($OH^{\cdot}$), and Eq. 4 to form superoxide radical ($O_2^{-\cdot}$). For this reason, Mo_6@LDH-2 with H_2O_2 presents a higher catalytic activity than Mo_6@LDH-2 with UV light. During the initiating process by Mo_6@LDH-2 with H_2O_2 and UV light, the Eq. 5 and Eq. 6 site reactions could significantly occur to reduce the H_2O_2. The degradation rates of the pollutants will decrease with the increase in the H_2O_2 concentration despite Eq. 7. The generated hydroxyl radical can randomly attack the MB organic compound by hydrogen abstraction, electron transfer, and radical combination to form the oxidation products [56].

The representation of the structure and activity mechanism of Mo_6@LDH-2 for the degradation of MB is illustrated in **Figure 8**. The efficiency of the catalytic activity depends on the generation of highly reactive radicals and the stability of the radicals. Without the light irradiation, ZnAl–LDH acts as a weak basic catalyst with the

hydroxide group the surface. ZnAl–LDH did not show the photocatalytic possibility due to the weak performance of the Zn metal in the photocatalytic reaction [39]. In addition, dye degradation was caused by the photocatalytic and oxidizing reactions. As a result, the catalytic property of the Mo_6@LDH-2 was mostly originated from the photoactive and oxidizing Mo metal cluster and the absorption caused by LDH. In the reduced form, the valence electron concentration (VEC) occupying in the d orbitals of the six Mo atoms, is equal to 24 electrons per Mo_6 cluster unit and it is reduced by a strong oxidizing agent [31]. Moreover, a chemically and an electrochemically reversible system has been reported. The Mo_6 cluster unit also provides one electron when excited by the light and transfer to O_2 to form singlet oxygen ($^{\cdot}O_1$) thus exhibiting a powerful oxidant property [30, 32]. It could be summarized in this study that i) the reducing form of the Mo_6 cluster can oxidize the MB molecules, ii) the Mo_6 cluster can combine with H_2O_2 to create powerful, oxidizing hydroxides ($OH^{\cdot}$), ii) the Mo_6 cluster can be excited by the UV light to form the hole and electron pair on the photoexcited cluster which reacts with H_2O molecules to create the $OH^{\cdot}$ radicals, and superoxide radical ($O_2^{-\cdot}$), particularly, singlet oxygen ($^{\cdot}O_1$) as a powerful oxidant caused by photoluminescence [36,37,38]. The oxygen-based radicals will first attack the C=S+-C linking of the MB molecule existing on the surface of the LDH. A degradation mechanism of MB caused by the oxygen-based radical is reported to form hydroxylation and oxidation products in a previous study [57]. To understand the impact of the UV light on the catalytic reaction, we consider some possible reasons. The UV light at 370 nm was used with the purpose to optimally create the $^{\cdot}O_1$, $O_2^{-\cdot}$ and $OH^{\cdot}$ oxygen-based radicals on the Mo_6 cluster which directly react with MB. Unfortunately, from Figure 3, the UV light at 370 nm is partially absorbed by the Zn-Al hydroxide layers that cause the decrease of the excitation photon

used for the Mo_6 cluster. In addition, the hole in the photoexcited Mo_6 cluster also reacts with water to form protons which reduce the concentration of the $OH^{\cdot}$ radicals. In the catalyst with the H_2O_2/UV system, the H_2O_2 molecules could be degraded by the UV energy. For this reason, the UV light will negatively affect the MB reducing the efficiency of the Mo_6 cluster when UV light and H_2O_2 are used at the same time. In summary, the prominent catalytic activity of the Mo_6 cluster stabilized on ZnAl-LDH has been confirmed. The combination of the LDH with high absorbability and the recyclability and the chemically reserving Mo_6 cluster will be a promising candidate as a homogeneous catalyst for gas reactions with a strong selection based on the layer structure.

4. CONCLUSIONS

A heterogeneous nanocomposite of ZnAl-LDH functionalized with the molybdenum octahedral cluster (~ 16.7 wt. %) was successfully synthesized by the precipitation and anion exchanging method under ambient conditions. The partially exfoliated ZnAL-LDH functionalized with the Mo_6 cluster was carried out. The interaction between the Mo_6 clusters and ZnAl-LDH is suggested to be via hydrogen bonding and/or new Mo-O-Al/Zn covalent linkage. The photoactive and oxidation of the Mo_6 cluster in the Mo_6@LDH nanocomposite present the important role to degrade methylene blue (MB). This point was investigated under UV (λ = 370 nm), in the presence of H_2O_2, or both of UV and H_2O_2 as radical initial agents. The efficiency of the degradation of MB using the Mo_6@LDH-2 nanocomposite is evaluated at more than about 90 wt% after 2 h with H_2O_2 as optimal co-agent. These results proved that the octahedral Mo_6 clusters are efficiently retained on the brucite-like layers that provide new heterogeneous catalytic

materials' family for gas reactions in the future.

ACKNOWLEDGMENT

These studies were carried out as a part of the France-Japan International Collaboration Framework (UMI3629 LINK). The authors wish to thank Mr. D. Lechevalier and Dr. M. Zhou of Saint-Gobain KK (Tokyo, Japan) and Dr. D. Berthebaud of CNRS for their many supports involved in LINK and related activities. We also wish to thank Dr. C. Zhang at NIMS for his help with the EPD experiments, Dr. A. Iwanade at NIMS for his help with the ICP-OES measurement and Dr. H. Ohata at NIMS for his help with the XPS measurements.

APPENDIX A. SUPPLEMENTARY MATERIAL

Supplementary data to this article can be found online at

REFERENCES

1. Pirila, M., Drault, F., Keiski, R.L., Saouabe, M., Valtanen, A., Ojala, S., Huuhtanen, M., Rathnayake, B., Brahmi, R., 2015. Photocatalytic Degradation of Organic Pollutants in Wastewater. Top Catal. 58, 1085-1099.

2. Bagheri, S., Yousefi, A.T., Do, T.O., 2017. Photocatalytic pathway toward degradation of environmental pharmaceutical pollutants: structure, kinetics and mechanism approach, Catal. Sci. Technol., 7, 4548–4569.

3. Fanourakis, S.K., Peña-Bahamonde, J., Bandara, P.C., Rodrigues, D.F., 2020. Nano-based adsorbent and photocatalyst use for pharmaceutical contaminant removal during

547 indirect potable water reuse, npj Clean Water, 3, 1-15.
548 4. Mohapatra, L., Parida, K., 2016. A review on the recent progress, challenges and
549 perspective of layered double hydroxides as promising photocatalysts, J. Mater. Chem.
550 A, 4, 10744-10766.
551 5. Chubar, N., Gilmour, R., Gerda, V., Mičušík, M., Omastova, M., Heister, K., Man, P.,
552 Fraissard, J., Zaitsev, V., 2017. Layered double hydroxides as the next generation
553 inorganic anion exchangers: Synthetic methods versus applicability, Adv. Colloid and
554 Inter. Sci. 245, 62-80.
555 6. Meng, Z., Zhang, Y., Zhanga, Q., Chena, X., Liua, L., Komarneni, S., Lva, L., 2017.
556 Novel synthesis of layered double hydroxides (LDHs) from zinc hydroxide, App. Surf.
557 Sci. 396, 799-803.
558 7. Ahmed, A. A. A., Tali, Z. A., Hussein, M. Z., Zakaria, A., 2012. Zn–Al layered double
559 hydroxide prepared at different molar ratios: Preparation, characterization, optical and
560 dielectric properties, J. Solid State Chem. 191, 271-278.
561 8. Kim, S. J., Lee, Y., Lee, D. K., Lee, J. W., Kang, J.K., 2014. Efficient Co–Fe layered
562 double hydroxide photocatalysts for water oxidation under visible light, J. Mater. Chem.
563 A, 2, 4136-4139.
564 9. Chowdhury, P. R., Bhattacharyya, K. G., 2015. Synthesis and characterization of
565 Co/Ti layered double hydroxide and its application as a photocatalyst for degradation of
566 aqueous Congo Red, RSC Adv. 5, 92189-92206.
567 10. Zheng, Y., Chen, Y., 2017. Preparation of polypropylene/Mg–Al layered double
568 hydroxides nanocomposites through wet pan-milling: formation of a second-staging
569 structure in LDHs intercalates. RSC Adv. 7, 1520-1530.
570 11. Fu, Y., Ning, F., Xu, S., An, H., Shao, M., Wei, M., 2016. Terbium doped ZnCr-

571 layered double hydroxides with largely enhanced visible light photocatalytic
572 performance, J. Mater. Chem. A 4, 3907-3913.
573 12. Ma, L., Wang, Q., Islam, S. M., Liu, Y., Ma, S., Kanatzidis, M. G., 2016. Highly
574 selective and efficient removal of heavy metals by layered double hydroxide
575 intercalated with the MoS_4^{2-} ion, J. Am. Chem. Soc. 138, 2858−2866.
576 13. Fan, G., Li, F., Evans, D. G., Duan, X. 2014. Catalytic applications of layered
577 double hydroxides: recent advances and perspectives, Chem. Soc. Rev. 43, 7040-7066
578 14. Wu, M. J., Wu, J. Z., Zhang, J., Chen, H., Zhou, J. Z., Qian, G. R., Xu, Z. P., Dud, Z.,
579 Rao, Q. L., 2018. A review on fabricating heterostructures from layered double
580 hydroxides for enhanced photocatalytic activities, Catal. Sci. Technol. 8,1207-1228.
581 15. Patel, R., Park, J. T., Patel, M., Dash, J. K., Gowd, E. B., Karpoormath, R., Mishra,
582 A., Kwak, J., Kim, J. H., 2018. Transition-metal-based layered double hydroxides
583 tailored for energy conversion and storage, J. Mater. Chem. A 6, 12-29.
584 16. Barahuie, F., Hussein, M.Z., Arulselvan, P., Fakurazi, S., Zainal, Z., 2014. Drug
585 delivery system for an anticancer agent, chlorogenate-Zn/Al-layered double hydroxide
586 nanohybrid synthesised using direct co-precipitation and ion exchange methods, J. Solid
587 State Chem. 217, 31-41.
588 17. Fontes, D.A.F., Lyra, M.A.M., Andrad, J. K. F., Schver, G. C. R., Rolim, L.A., Silva,
589 T. G., Soares-Sobrinho, J.L., Alves-Junior, S., Rolim-Neto, P.J., 2016. CaAl-layered
590 double hydroxide as a drug delivery system: effects on solubility and toxicity of the
591 antiretroviral efavirenz, J. Incl. Phenom. Macrocycl. Chem., 85, 281-288.
592 18. Kura, A.U., Hussein, M.Z., Fakurazi, S., Arulselvan, P., 2014. Layered double
593 hydroxide nanocomposite for drug delivery systems; bio-distribution, toxicity and drug
594 activity enhancement, Chem. Central J. 8, 47-55.

595 19. Sahoo, M., Singha, S., Parida, K. M., 2011. Amine functionalized layered double
596 hydroxide: a reusable catalyst for aldol condensation, New J. Chem. 35, 2503-2509.
597 20. Shao, M., Ning, F., Zhao, J., Wei, M., Evans, D.G., Duan, X., 2013. Hierarchical
598 layered double hydroxide microspheres with largely enhanced performance for ethanol
599 electrooxidation, Adv. Funct. Mater. 23, 3513-3518.
600 21. Zhao, Y., Zhao, Y., Waterhouse, G. I .N., Zheng, L., Cao, X., Teng, F., Wu, L. Z.,
601 Tung, C.H., O'Hare, D., Zhang, T., 2017. Layered-Double-Hydroxide nanosheets as
602 efficient visible-light-driven photocatalysts for dinitrogen fixation, Adv. Mater. 29,
603 1703828-1703838.
604 22. Zhang, j., Liu, J., Xi, L., Yu, Y., Ning Chen, .N, Sun, S., Wang, W., Lange, K.M.,
605 Zhang, B., 2018. Single-Atom Au/NiFe Layered Double Hydroxide Electrocatalyst:
606 Probing the Origin of Activity for Oxygen Evolution Reaction, J. Am. Chem. Soc., 140,
607 3876−3879.
608 23. Iqbal, K., Iqbal, A., Kirillov, A.M., Wang, B., Liu, W., Tang, Y., 2017. A new Ce-
609 doped MgAl-LDHs@Au nanocatalyst for highly efficient reductive degradation of
610 organic contaminants. J. Mater. Chem. A, 5, 6716 –6724.
611 24. Liu, J.C., Qi, B., Song, I.F., 2020, Engineering polyoxometalate-intercalated layered
612 double hydroxides for catalytic applications, Dalton Trans., 49, 3934–3941.
613 25. Cotton, F.A., 1964. Metal Atom Clusters in Oxide Systems. Inorg. Chem. 3, 1217-
614 1220.
615 26. Nguyen, T. K. N., Renaud, A., Bierre, B., Bouteille, B., Wilmet, M., Dubernet, M.,
616 Ohashi, N., Grasset, F., Uchikoshi, T. Extended Study on Electrophoretic Deposition
617 Process of Inorganic Octahedral Metal Clusters: Advanced Multifunctional Transparent
618 Nanocomposite Thin Films, Bull. Chem. Soc. Jpn., 2018, 91, 1763-1774.

27. Neaime, C., Amela-Cortes, M., Grasset, F., Molard, Y., Cordier, S., Dierre, B., Mortier, M., Takei, T., Takahashi, K., Haneda, H., Verelst, M., Lechevallier, S., 2016. Time-gated luminescence bioimaging with new luminescent nanocolloids based on $[Mo_6I_8(C_2F_5COO)_6]^{2-}$ metal atom clusters, Phys. Chem. Chem. Phys. 18, 30166-30173.

28. Efremova, O.A., Brylev, K.A., Vorotnikov, Y.A., Vejsadova, L., Shestopalov, M.A., Chimonides, G.F, Mikes, P., Topham, P.D., Kim, S.J., Kitamurah, N., Sutherland, A.J., 2016. Photoluminescent materials based on PMMA and a highly-emissive octahedral molybdenum metal cluster complex. J. Mater. Chem. C, 4, 497-503.

29. Kirakci, K., Kubát, P., Dusek, M., Fejfarová, K., Sícha, V., Mosinger, J., Lang, K., 2012. A Highly Luminescent Hexanuclear Molybdenum Cluster–A Promising Candidate toward Photoactive Materials, Eur. J. Inorg. Chem. 19, 3107-3111.

30. Kirakci, K., Kubát, P., Langmaier, J., Polívka, T., Fuciman, M., Fejfarovád, K., Lang, K.A., 2013. Comparative study of the redox and excited state properties of $(nBu_4N)_2[Mo_6X_{14}]$ and $(nBu_4N)_2[Mo_6X_8(CF_3COO)_6]$ (X = Cl, Br, or I), Dalton Trans. 42, 7224-7232.

31. Vorotnikova, N.A., Vorotnikov, Y.A., Novozhilov, I. N., Syrokvashin, M.M., Nadolinny, V.A., Kuratieva, N.V., Benoit, D.M., Mironov, Y.V., Walton, R.I., Clarkson, G.J., Kitamura, N., Sutherland, A.J., Shestopalov, M.A., Efremova, O.A., 2018. ^{23}Electron Octahedral Molybdenum Cluster Complex $[\{Mo_6I_8\}Cl_6]^{-}$, Inorg. Chem. 57, 811−820.

32. Costuas, K., Bulou, A.A., Fontaine, B., Cuny, J., Gautier, R., Mortier, M., Molard, Y., Duvail, J.L., Faulques, E., Cordier, S., 2015. Combined theoretical and time-resolved photoluminescence investigations of $[Mo_6Br^{i}_8Br^{a}_6]$ metal cluster units: evidence of dual emission, Phys. Chem. Chem. Phys. 17, 28574-28585.

643 33. Jackson, J.A., Turro, C., Newsham, M.D., Nocera, D.G., 1990. Oxygen Quenching
644 of Electrontcally Excited Hexanuclear Mdybdenum and Tungsten Halide Clusters, J.
645 Phys. Chem. A. 94, 4500-4507.
646 34. Feliz, M., Puche, M., Atienzar, P., Concepciûn, P., Cordier, S., Molard, Y., 2016. In
647 Situ Generation of Active Molybdenum Octahedral Clusters for Photocatalytic
648 Hydrogen Production from Water, Chem. Sus. Chem. 9, 1963-1971.
649 35. Ivanova, M.N., Vorotnikov, Y.A., Plotnikova, E.E., Marchuk, V.M., Ivanov, A.A.,
650 Asanov, I.P., Tsygankova, A.R., Grayfer,E.D., Fedorov, V.E., Shestopalo, M.A., 2020,
651 Hexamolybdenum Clusters Supported on Exfoliated h-BN Nanosheets for
652 Photocatalytic Water Purification, Inorg. Chem., 59, 6439-6448.
653 36. Kumar, S., Khatri, O. P., Cordier, S., Boukherroub, R., Jain, S.L., 2015. Graphene
654 Oxide Supported Molybdenum Cluster: First Heterogenized Homogeneous Catalyst for
655 the Synthesis of Dimethylcarbonate from CO_2 and Methanol, Chem. Eur. J. 21, 3488 -
656 3494.
657 37. Barras, A., Devarapallic, M.R., Shelkec, R.R., Cordier, S., M.V., Szunerits, S.,
658 Boukherroub, R., 2013. One-pot synthesis of gold nanoparticle/molybdenum
659 cluster/graphene oxide nanocomposite and its photocatalytic activity, App. Cat. B: Envi.
660 270- 276, 130-131.
661 38. Barras, A., Cordier, S., Boukherroub, R., 2012. Fast photocatalytic degradation of
662 rhodamine B over $[Mo_6Br_8(N_3)_6]^{2-}$ cluster units under sun light irradiation, Appl. Cat.
663 B: Envi. 123-124, 1- 8.
664 39. Yang, Y., Zhang, C., Zeng, G., Tan, X., Wang, H., Huang, D., Yang, K., Wei, J.,
665 Maab, C., Niec, K., 2020. Design and engineering of layered double hydroxide based
666 catalysts for water depollution by advanced oxidation processes: a review, J. Mater.

667 Chem. A 8, 4141–4173.
668 40. Starukh, G., 2017. Photocatalytically enhanced cationic dye removal with Zn-Al
669 layered double hydroxides. Nanoscale Research Lett. 12, 391-399.
670 41. Saito, N., Lemoine, P., Dumait, N., Amela-Cortes, M., Paofai, S., Roisnel, T., Nassif,
671 V., Grasset, F., Wada, Y., Ohashi, N., Cordier, S., 2017. From $Cs_2Mo_6Cl_{14}$ to
672 $Cs_2Mo_6Cl_{14}$ center dot H_2O and Vice Versa: Crystal Chemistry Investigations, J. Clust.
673 Sci. 28, 773-798.
674 42. Kirakci, K., Cordier, S., Perrin, C., 2005. Synthesis and characterization of
675 $Cs_2Mo_6X_{14}$ (X = Br or I) hexamolybdenum cluster halides: Efficient Mo_6 cluster
676 precursors for solution chemistry syntheses. Z. Anorg. Allg. Chem. 631, 411-416.
677 43. Deng, L., Zeng, H., Zhang, Z.W., Luo, J., Sodium dodecyl sulfate intercalated and
678 acrylamide anchored layered double hydroxides: A multifunctional adsorbent for highly
679 efficient removal of Congo red. J. Colloid and Inter. Sci. 521 (2018) 172-182.
680 44. Ahmed, A.A.A., Talib, Z.A., Hussein, M.Z., 2015. Influence of sodium dodecyl
681 sulfate concentration on the photocatalytic activity and dielectric properties of
682 intercalated sodium dodecyl sulfate into Zn–Cd–Al layered double hydroxide, Mater.
683 Research Bulletin. 62, 122-131.
684 45. Zarate, X., Schott, E., Soto, L.A., Tagle, R.R., 2013. A family of octahedral
685 molybdenum cluster complexes $[Mo_6Cl_8(H_2O)_n(OH)_{6-n}]^{n-2}$ with n = 0–6 as a pH-
686 sensors: A theoretical study, Chem. Phys. Lett. 567, 39-42.
687 46. Chuntonov, L., Kumar, R., Kuroda, D.G., 2014. Non-linear infrared spectroscopy of
688 the water bending mode: direct experimental evidence of hydration shell reorganization.
689 Chem. Chem. Phys., 16, 13172-13181.
690 47. Nguyen, T.K.N., Dierre, B., Grasset, F., Renaud, A., Cordier, S., Lemoine, P.,

691 Ohashi, N., Uchikoshi, T. 2017. Formation mechanism of transparent Mo_6 metal atom
692 cluster film prepared by electrophoretic deposition, J. Electrochem. Soc., 164, 412-418.
693 48. Richetta, M., Digiamberardino, L., Mattoccia, A., Medaglia, P.G., Montanari, R.,
694 Pizzoferrato, R., Scarpellini, D., Varone, A., Kaciulis, S., Mezzi, A., Soltania, P., Orsinid,
695 A., 2016. Surface spectroscopy and structural analysis of nanostructured multifunctional
696 (Zn, Al) layered double hydroxides, Surf. Interface Anal. 48, 514-518.
697 49. Galtayries, A., Wisniewski, S., Grimblot, J., 1997. Formation of thin oxide and
698 sulphide films on polycrystalline molybdenum foils: characterization by XPS and
699 surface potential variations. J. Electron Spectroscopy and Related Phenomena, 87, 31-
700 44.
701 50. Castañeda, S.I., Montero, I., Ripalda, J.M., Díaz, N., Galán, L., Rueda, F., 1999. X-
702 ray photoelectron spectroscopy study of low-temperature molybdenum oxidation
703 process, J. Appl. Phys. 85, 8415-8418.
704 51. Bamroongwongdee, C., Bowker, C. M.A.F., Davies, P. R., Davies, R. J., Edwards,
705 D., 2013. Fabrication of complex model oxide catalysts: Mo oxide supported on
706 Fe_3O_4(111), Faraday Discuss, 162, 201–212.
707 52. Li, H., Deng, Q., Liu, L., Hou, W., Du, N., Zhang, R., Tao, X., 2014. Synthesis,
708 characterization and enhanced visible light photocatalytic activity of Bi_2MoO_6/Zn–Al
709 ed double hydroxide hierarchical heterostructures, Catal. Sci. Technol. 4, 1028–1037.
710 53. Saito, N., Cordier, S., Lemoine, P., Ohsawa, T., Wada, Y., Grasset, F., Cross, J. S.,
711 Ohashi, N., 2017. Lattice and valence electronic structures of crystalline octahedral
712 molybdenum halide clusters-based compounds, $Cs_2[Mo_6X_{14}]$ (X = Cl, Br, I), studied by
713 density functional theory calculations, Inorg. Chem. 56, 6234−6243.
714 54. Tijani, J.O., Fatoba, O.O., Madzivire, G., Petrik, L.F., 2014. A review of combined

advanced oxidation technologies for the removal of organic pollutants from water. Water, Air, Soil & Pollution, 225, 2102-2148.

55. Gligorovski, S., Strekowski, R., Barbati, S., Vione, D., 2015. Environmental implications of hydroxyl radicals (•OH). Chem. Rev., 115, 13051−13092.

56. Munter, R., 2001. Advanced oxidation processes – current status and prospects. Proc. Estonian Acad. Sci. Chem. 50, 59-80.

57. Xia, S., Zhang, L., Pan, G., Qiana, P., Ni, Z., 2015. Photocatalytic degradation of methylene blue with a nanocomposite system: synthesis, photocatalysis and degradation pathways. Phys. Chem. Chem. Phys., 17, 5345-535.

FIGURE CAPTIONS

Figure 1. A) Powder-XRD patterns of LDH-1, Mo_6@LDH-1, LDH-2, Mo_6@LDH-2 with the indications of the planes of 003 (■), 006 (●), 009 (▲) and the lozenge symbol (♦) assigned for the ZnO phase. B) The schematic representation of the process to fabricate the LDH and designed structure of its nanocomposite.

Figure 2. A) The HR-TEM, B) STEM images of the layered structure, and C) profile of spacing distance between the layers, and D) STEM-EDX mapping of the Mo_6@LDH-2 nanocomposite.

Figure 3. A) UV-Vis absorbance spectra and B) room temperature photoluminescence spectra excited by 325 nm (He-Cd) laser of CMC cluster, LDH-1, LDH-2, and Mo_6@LDH-2.

Figure 4. FTIR spectra of CMC cluster and Mo_6@LDH nanocomposites.

Figure 5. Thermal analysis of LDH-1, LDH-2, and Mo6@LDH-2

Figure 6. (A) XPS binding energy (eV) spectrum of the CMC powder and the

739 Mo_6@LDH-2 nanocomposite, XPS spectra of (B) Mo 3d, (C) Cl 2p region.
740 Deconvolution spectra of Cl 2p region of (D) the CMC and (E) Mo_6@LDH-2.
741 **Figure 7**. A) The MB-degradable possibility caused by (1) Mo_6 cluster, (2) Mo_6@LDH-
742 2, and (3) LDH-2 without and with H_2O_2 during stirring for 2 h, B) the degradation rate
743 and C) the effect of H_2O_2 concentrations on MB-degradable possibility by Mo_6@LDH-2
744 for 210 minutes with and without UV light (λ=370 nm) illumination.
745 **Figure 8**. Schematic representation of the heterogeneous activation mechanism of
746 Mo_6@LDH-2 initialed by UV (λ=370 nm) and H_2O_2 oxidation agents.
747
748
749 **TABLES**
750 Table 1. XPS binding energy (eV) of deconvolution spectra of Cl 2p region of the
751 $[Mo_6Cl^i_8Cl^a_6]^2$ anions of CMC cluster and Mo_6@LDH-2.
752 Table 2. The concentration of the component elements in the CMCpowder and the
753 Mo_6@LDH-2 nanocomposite by the peak analysis of the XPS measurements.

Graphical Abstract

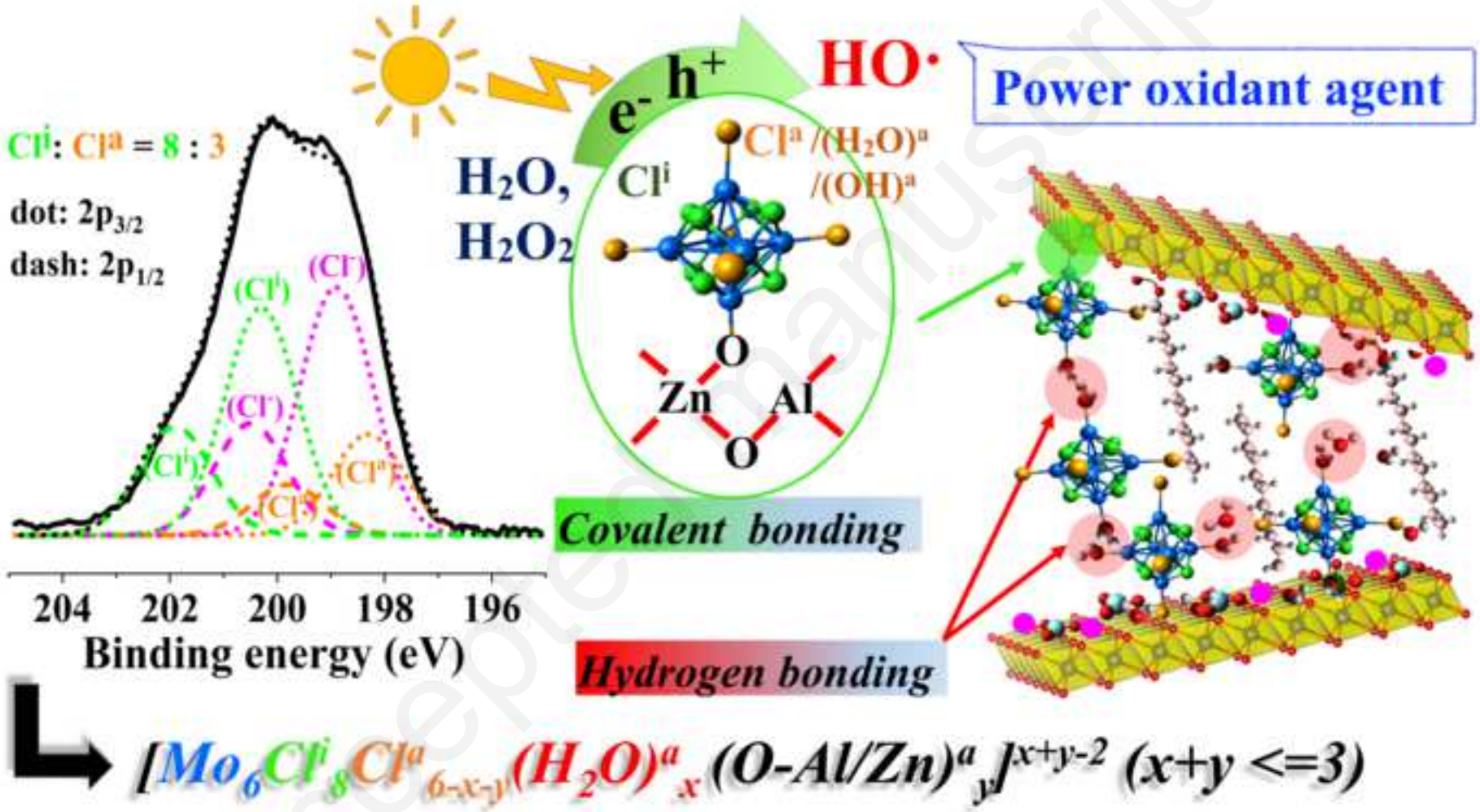

Highlights

ZnAl-LDHs were successfully functionalized with the hexamolybdenum cluster by covalent linkage.

A Mo_6@LDHs nanocomposite retains the photoactive and oxidation properties of the Mo_6 cluster

Three nanomaterial phases were found in the lamellar structure of the Mo_6@LDHs

H_2O_2/Mo_6@LDHs efficiently accelerated the degradation reaction of methylene blue with and without UV light illumination

TABLES

Table 1. XPS binding energy (eV) of deconvolution spectra of Cl 2p region of the $[Mo_6Cl^i_8Cl^a_6]^2$ anions of $Cs_2Mo_6Cl_{14}$ cluster and Mo_6@LDH-2.

Sample	B.E	FWHM	Height	% area	Peak	$Cl^i/Cl^a/Cl^{new}$
$Cs_2Mo_6Cl^i_8Cl^a_6$	198.25	1.15	15637	27.88	Cl $2p_{3/2}$ (a)	8/5.8/0
	199.85	1.15	7895	14.08	Cl $2p_{1/2}$ (a)	
	200.39	1.16	21005	37.78	Cl $2p_{3/2}$ (i)	
	201.99	1.16	11265	20.26	Cl $2p_{1/2}$ (i)	
Mo_6@LDH-2	198.25	1.6	977	11.90	Cl $2p_{3/2}$ (a)	8/3.6/8.6
	198.90	1.6	2403	28.28	Cl $2p_{3/2}$	
	199.85	1.6	488	5.95	Cl $2p_{1/2}$ (a)	
	200.35	1.6	2207	26.89	Cl $2p_{3/2}$ (i)	
	200.50	1.6	1081	13.17	Cl $2p_{1/2}$	
	201.95	1.6	1051	12.81	Cl $2p_{1/2}$ (i)	

Table 2. The concentration of the component elements in the $Cs_2[Mo_6Cl_{14}]$ powder and the Mo_6@LDH-2 nanocomposite by the peak analysis of the XPS measurements.

Element component (%at.)	$Cs_2Mo_6Cl_{14}$	Mo_6@LDH-2
Al	0	3.8
Zn	0	12.4
S	0	1.5
C	28.5	29.1
O	5.2	47.3
Cl	42	3.8
Mo	17.7	2.1

Cs	6.6	0
Cs/ Mo/Cl	2.2/6.0/14.2	0/6.0/10.7

Figure
Click here to download high resolution image

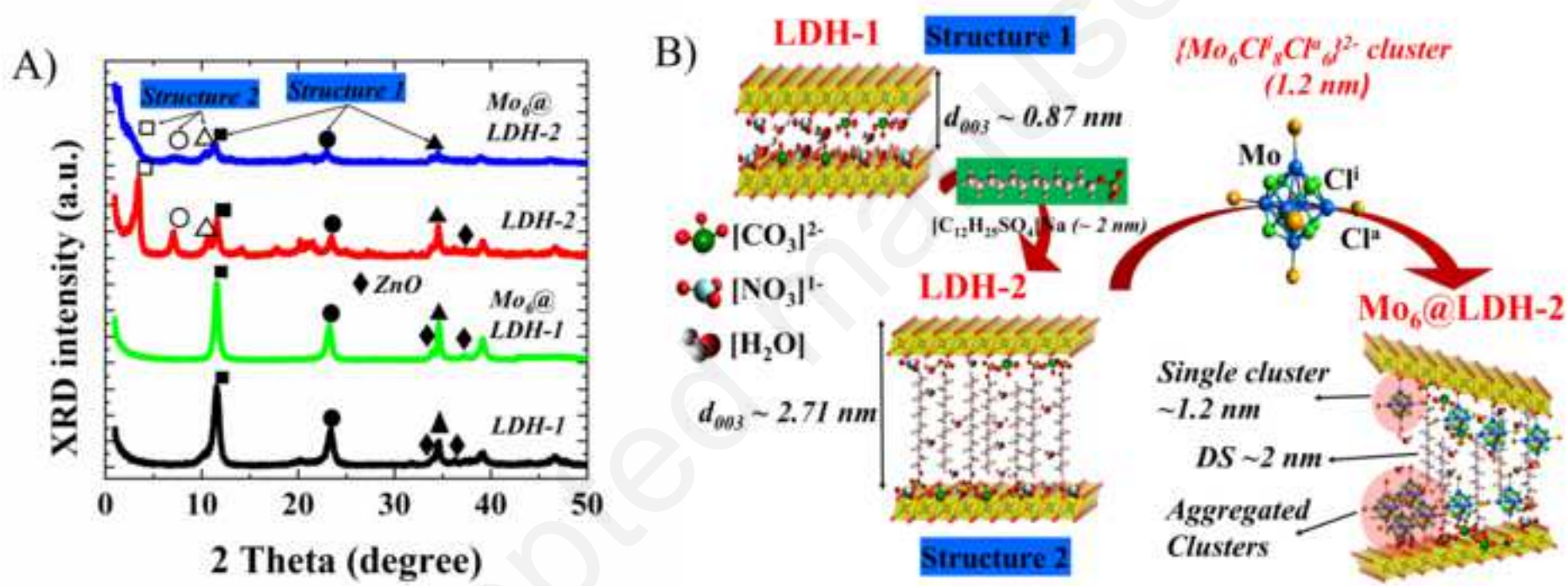

Figure

Click here to download high resolution image

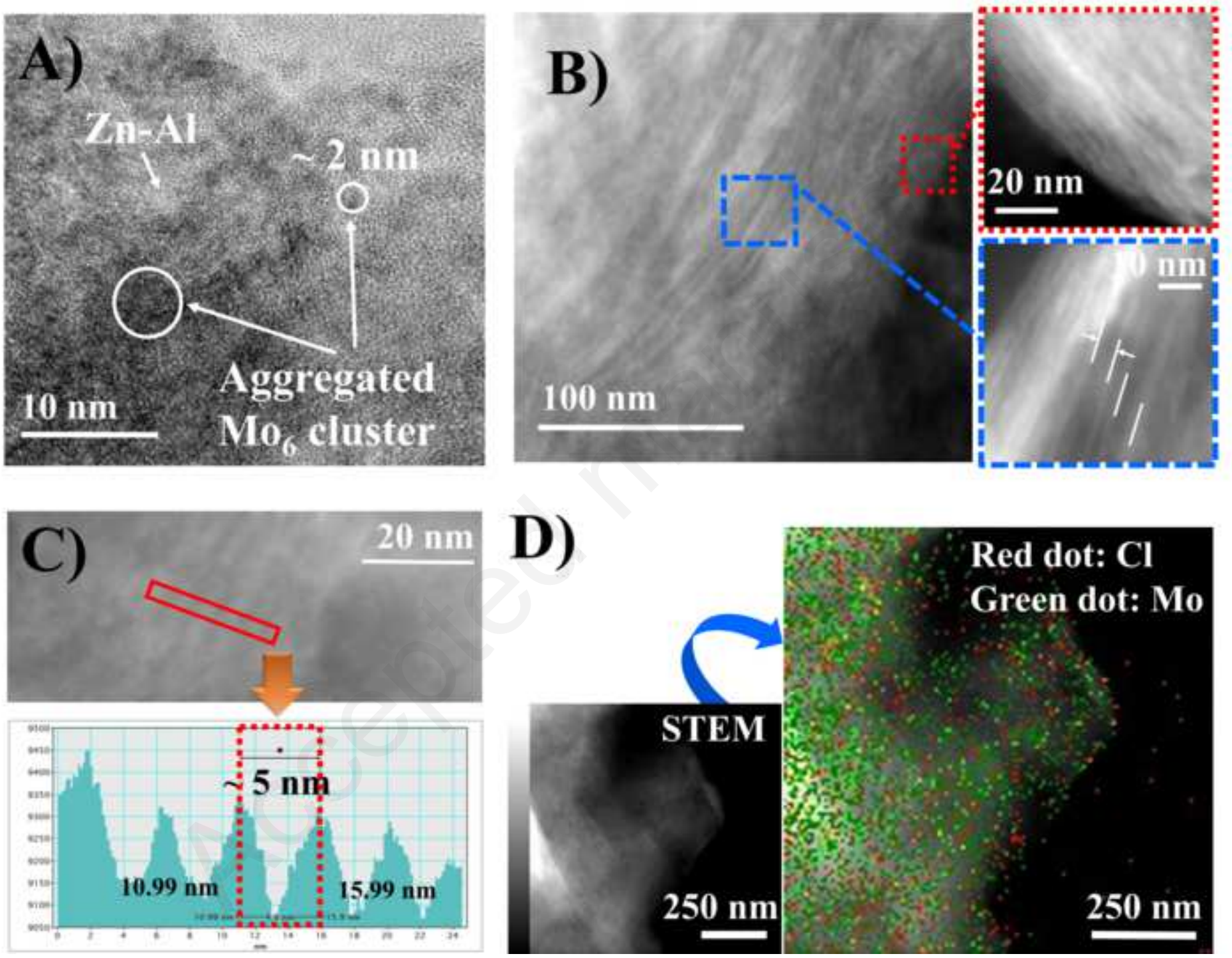

Figure

Click here to download high resolution image

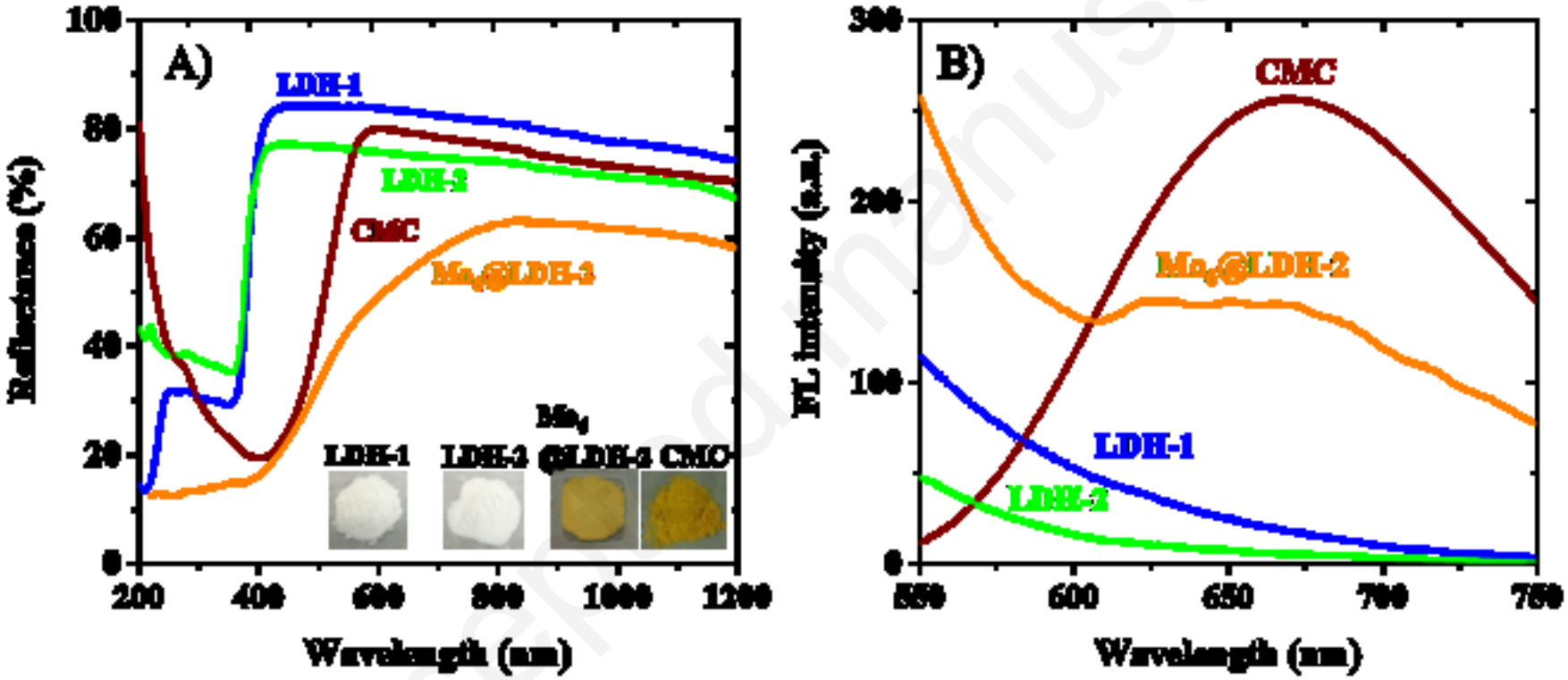

Figure
Click here to download high resolution image

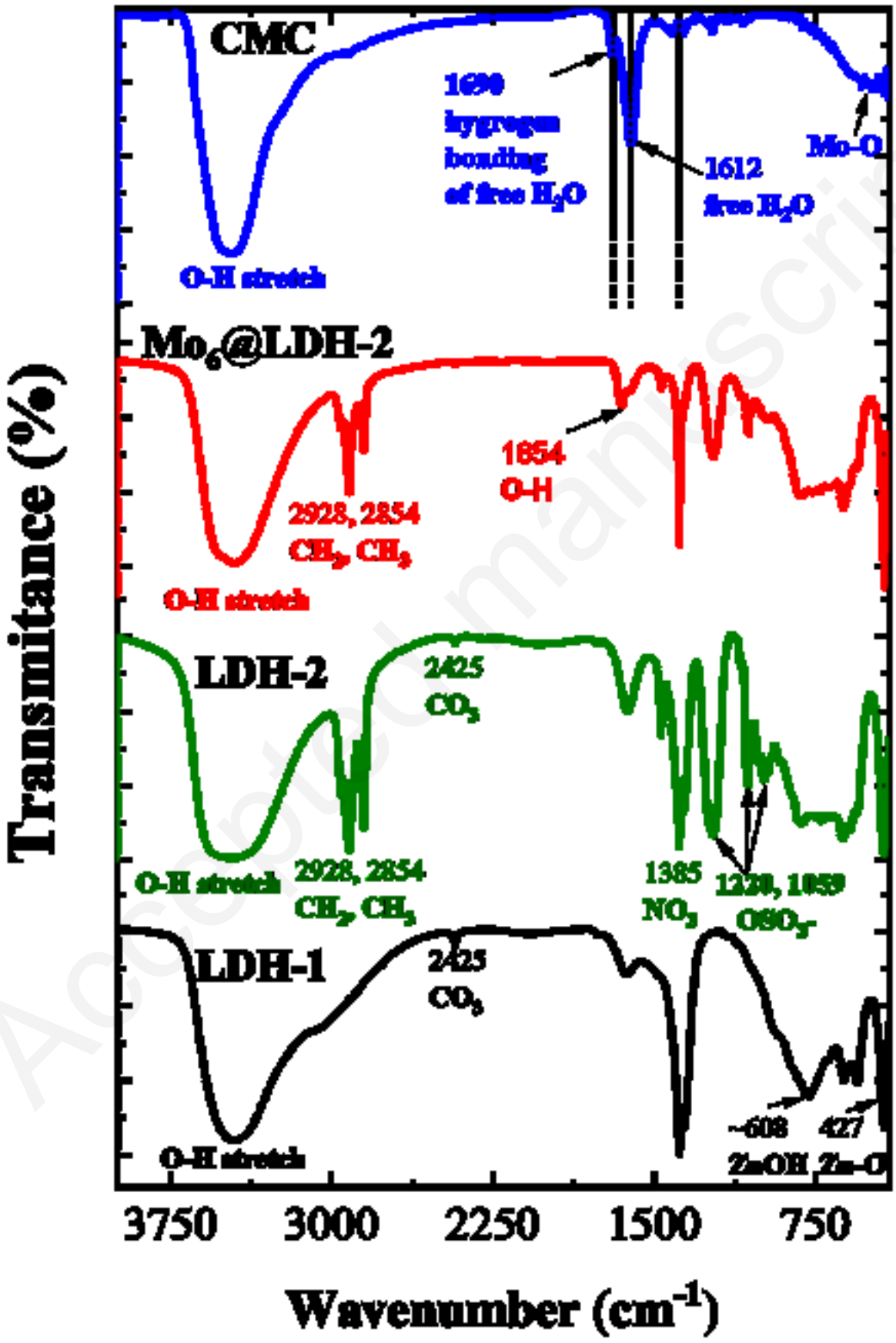

Figure
Click here to download high resolution image

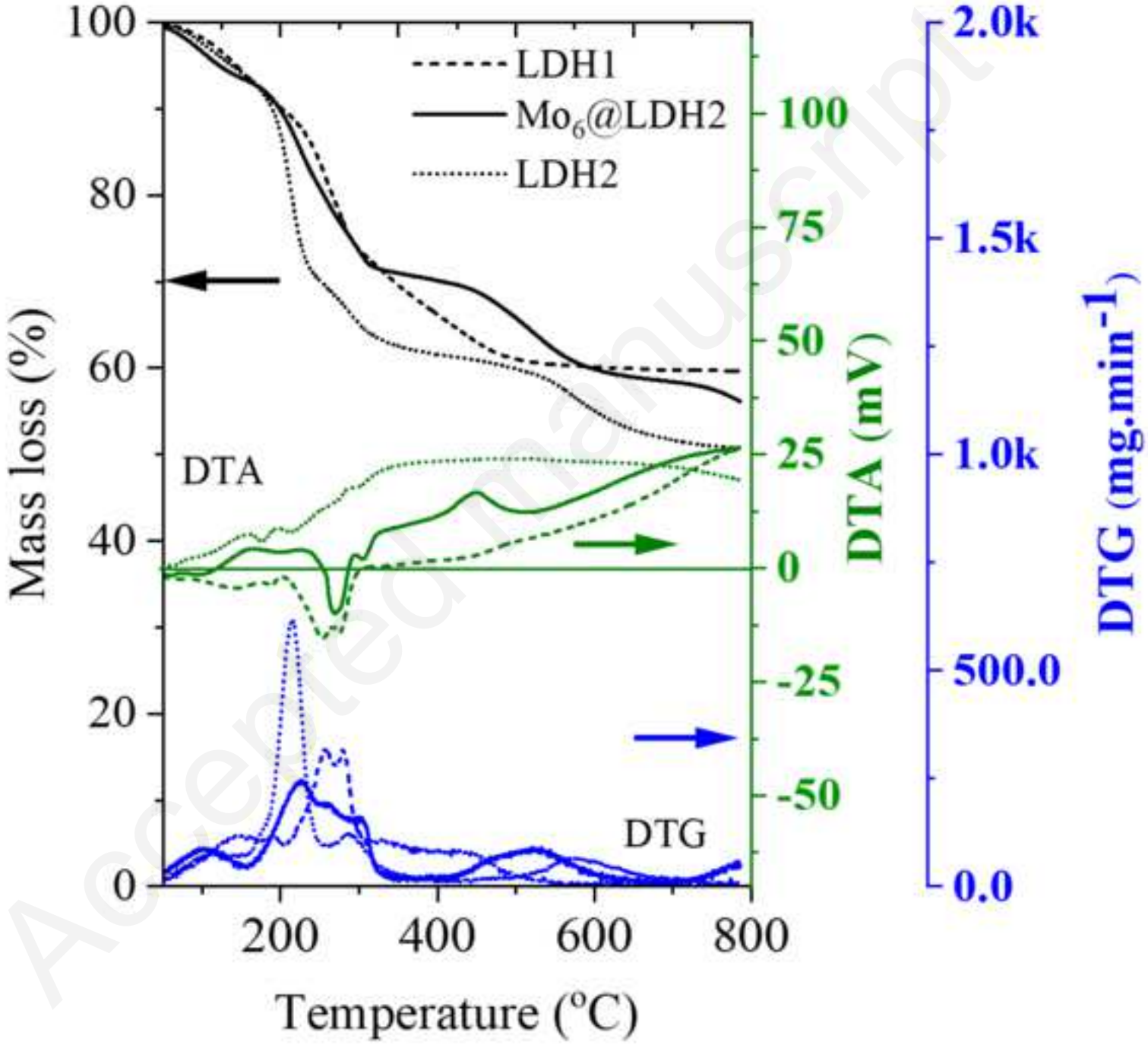

Figure

Click here to download high resolution image

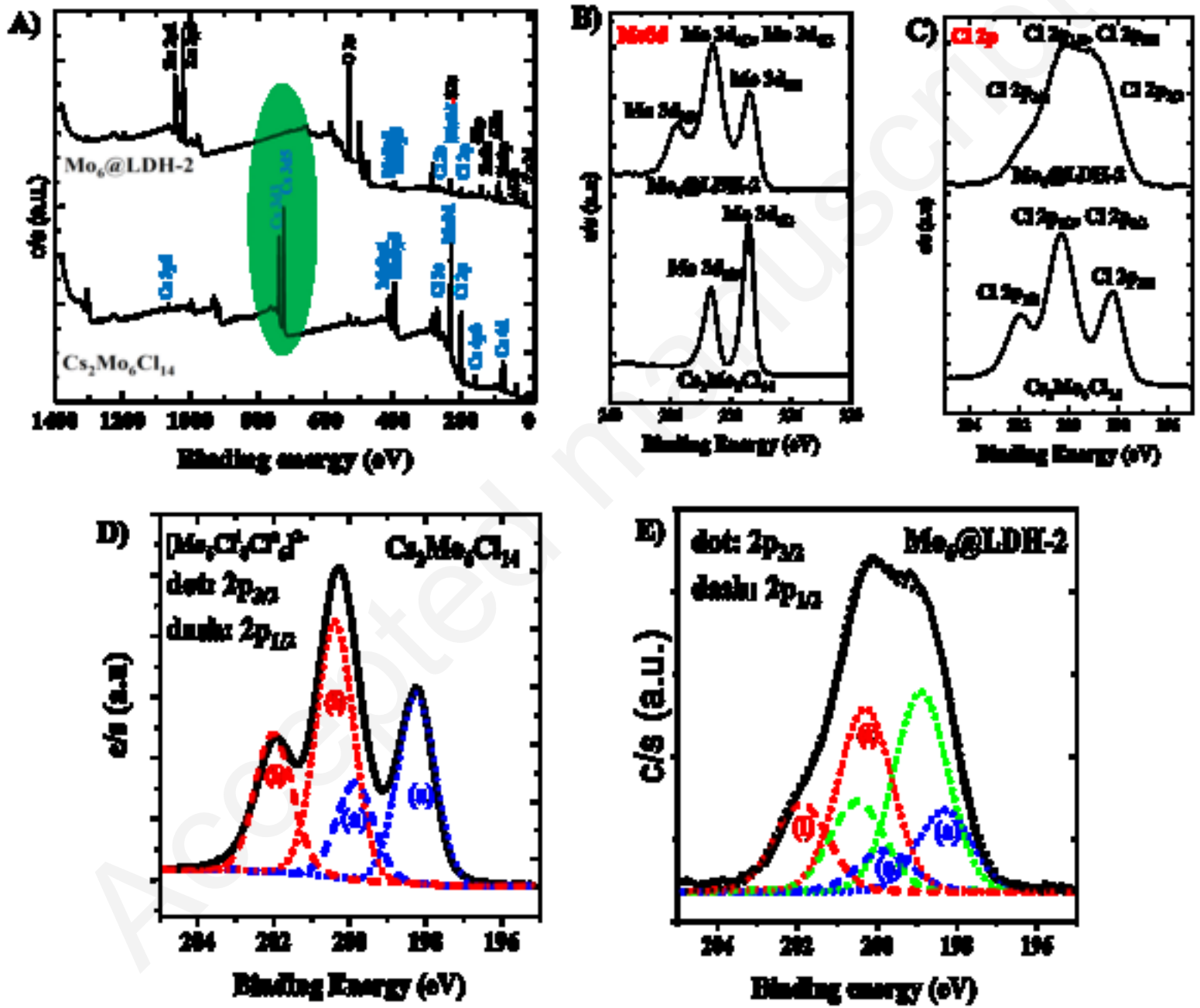

Figure

Click here to download high resolution image

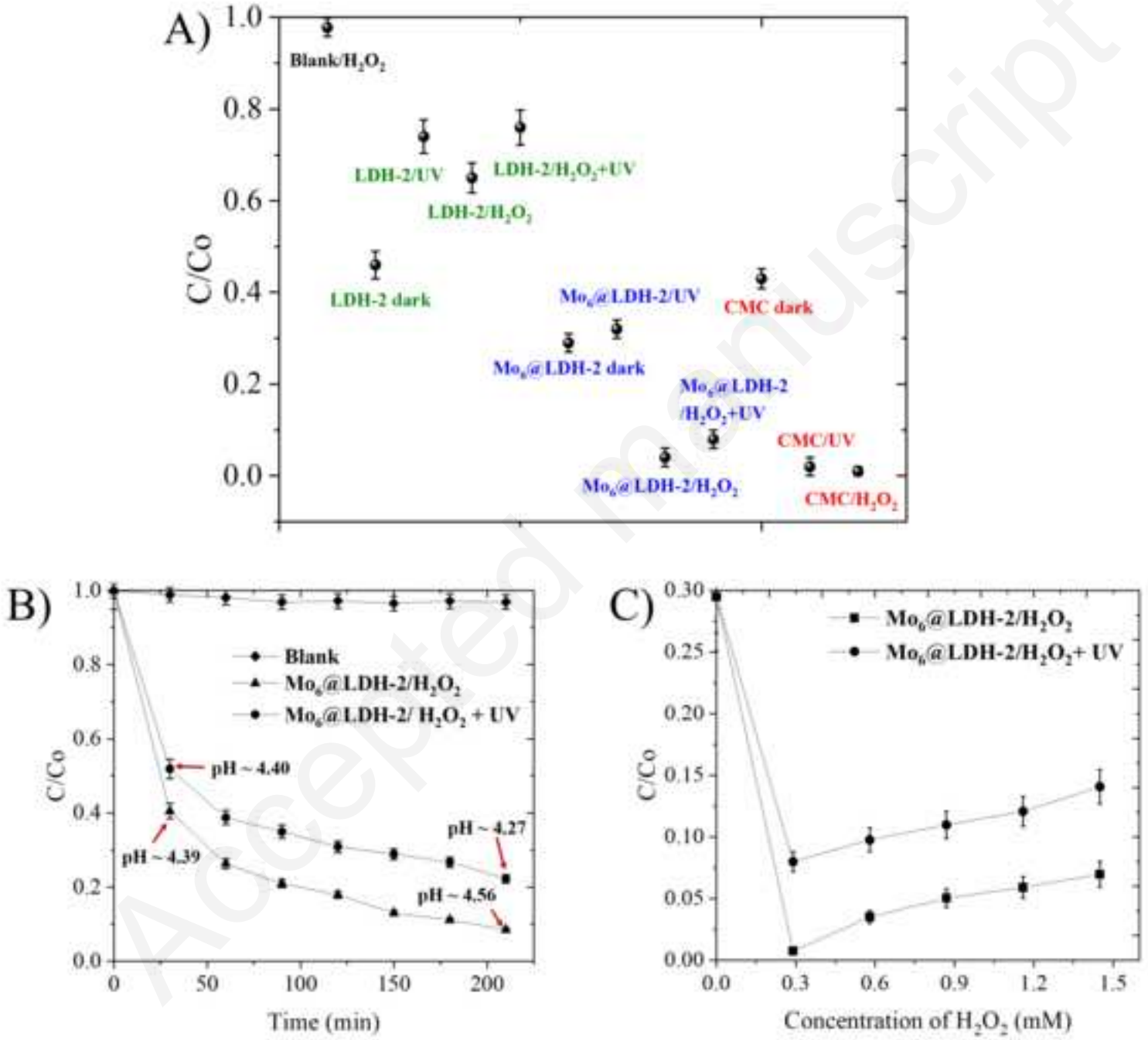

Figure

Click here to download high resolution image